AIAA 2001–2623

Multi-Dimensional Upwind Constrained Transport on Unstructured Grids for 'Shallow Water' Magnetohydrodynamics

Hans De Sterck [1,2,3]
[1]*von Karman Institute for Fluid Dynamics, Sint-Genesius-Rode, Belgium*
[2]*Centre for Plasma Astrophysics, Katholieke Universiteit Leuven, Belgium*
[3]*Department of Applied Mathematics, University of Colorado at Boulder, USA*

15th AIAA Computational Fluid Dynamics Conference
11 - 14 June 2001
Anaheim, California

Multi-Dimensional Upwind Constrained Transport on Unstructured Grids for 'Shallow Water' Magnetohydrodynamics

Hans De Sterck [1,2,3*]

[1] *von Karman Institute for Fluid Dynamics, Sint-Genesius-Rode, Belgium*

[2] *Centre for Plasma Astrophysics, Katholieke Universiteit Leuven, Belgium*

[3] *Department of Applied Mathematics, University of Colorado at Boulder, USA*

Novel Multi-dimensional Upwind Constrained Transport (MUCT) schemes on unstructured triangular grids are described. Constrained Transport (CT) discretizations conserve the divergence-free nature of divergence-free vector fields on the discrete level. Multi-dimensional Upwind (MU) schemes generalize the concept of dimensionally split upwind schemes for hyperbolic systems to truly multidimensional upwind discretizations on unstructured grids with compact stencils consisting of nearest neighbors. In the present paper the concept of Constrained Transport, generalized to unstructured triangular grids using face elements, is combined with the concept of Multi-dimensional Upwind advection schemes. The resulting MUCT schemes are applied to flow simulations on 2D triangular unstructured grids. The schemes are applied to the numerical solution of Faraday's law of induction in the Magnetohydropdynamic (MHD) approximation, which describes the dynamical evolution of a divergence-free magnetic field, and to the numerical solution of the the recently proposed hyperbolic system formed by the 'Shallow Water' Magnetohydrodynamics equations. It is described how the two-dimensional MUCT schemes presented can be generalized to flow simulation on three-dimensional tetrahedral grids. The MUCT schemes can be applied to any hyperbolic system with divergence-free fields, including the full MHD equations. In the MUCT schemes the CT approach is generalized to multi-dimensional methods on unstructured grids.

Introduction

Constrained Transport (CT) discretizations[1] conserve the divergence-free nature of advected divergence-free vector fields on the discrete level up to machine accuracy. CT discretizations are, e.g., attractive for simulations of physical systems involving the advection of magnetic fields, since it is an experimental fact that there exist no magnetic monopoles in nature, which is expresssed in the condition that the divergence of the magnetic field vanishes. CT discretizations mimic this physical property on the discrete level, which for some applications means that more accurate, more stable, or faster converging results can be obtained. Several variants of numerical schemes of CT type have been derived for Magnetohydrodynamic (MHD) simulations on logically structured curvi-linear grids[2–7] since CT schemes were introduced by Evans and Hawley in 1988.[1] Generalizations to unstructured grids have not been described in the literature.

Multi-dimensional Upwind (MU) residual distribution schemes generalize the concept of dimensionally split upwind schemes for hyperbolic systems to truly multidimensional upwind discretizations on unstructured grids with compact stencils consisting of nearest neighbors. They were proposed by Roe, Deconinck and co-workers,[8,9] and have extended their reach of application in recent years up to three-dimensional (3D) turbulent Navier-Stokes calculations[9,10] and 3D MHD calculations.[11]

In the present paper the concept of Constrained Transport, generalized to unstructured triangular grids using face elements, is combined with the concept of Multi-dimensional Upwind advection schemes. The resulting Multi-dimensional Upwind Constrained Transport (MUCT) schemes are applied to two-dimensional (2D) flows described by Faraday's equation and flows described by the recently proposed system of 'Shallow Water' Magnetohydrodynamics (SMHD).[12] The MUCT schemes can be applied to any hyperbolic system with divergence-free fields, including the full Magnetohydrodynamics (MHD) equations, and they can be generalized to 3D. In the MUCT schemes the CT approach is thus generalized to multi-dimensional methods on unstructured triangular or tetrahedral grids.

This paper is organized as follows.

In the first Section we present the background material necessary for the derivation of the MUCT schemes. Illustrated by the example of Faraday's equation, we discuss the general concept of Constrained Transport on unstructured grids. We provide a geometrical interpretation in terms of concepts from differen-

*Post–doctoral researcher; desterck@colorado.edu

tial geometry, and we describe the reconstruction of the cell magnetic field using face elements. A brief overview of Multi-dimensional Upwind residual distribution schemes is given.

In the second Section a class of Multi-dimensional Upwind Constrained Transport (MUCT) Schemes for Faraday's equation in 2D is proposed. We propose two different flavors of schemes, the first based on Multi-dimensional Upwind interpolation of the cell magnetic field towards the nodes, the second based on regular Multi-dimensional Upwind schemes for the scalar advection equation. The schemes are illustrated with simulations of smooth and discontinuous model flows.

The third Section discusses the extension of the MUCT schemes to the recently proposed 2D hyperbolic system of 'Shallow Water' Magnetohydrodynamics (SMHD)[12] that describes the dynamics of nearly incompressible conducting fluids for which the evolution is nearly two-dimensional with magnetohydrostatic equilibrium in the third direction. The novel SMHD equations are presently being used in the study of the dynamics of layers in the solar interior, but they may also be applicable to problems involving the free surface flow of conducting fluids in laboratory and industrial environments. The SMHD equations and their hyperbolic properties are briefly reviewed. MUCT schemes are then presented for the SMHD equations, and they are tested on a steady flow with a shock, a contact discontinuity and a rarefaction wave. The numerical divergence errors present in simulation results obtained by a traditional non-CT Multi-dimensional Upwind residual distribution scheme, a non-CT finite volume scheme, and the new MUCT scheme are compared.

Multi-Dimensional Upwind Constrained Transport

Constrained Transport on unstructured grids

In the present Section we intend to describe various ways in which the evolution Equation for the magnetic field $\vec{B}$ given by

$$\frac{\partial \vec{B}}{\partial t} = \nabla \times (\vec{v} \times \vec{B}), \tag{1}$$

with

$$\nabla \cdot \vec{B} = 0, \tag{2}$$

can be solved numerically.

This Equation can be derived from Faraday's law $\partial \vec{B}/\partial t = -\nabla \times \vec{E}$ in the approximation of a perfectly conducting MHD plasma flowing with velocity $\vec{v}$, for which the electrical field $\vec{E}$ is given by $\vec{E} = -\vec{v} \times \vec{B}$. In the present and following Sections we assume that the plasma velocity $\vec{v}$ is constant in space and time, a condition to be relaxed in the Section on MUCT schemes for the SMHD equations.

The divergence constraint Eq. 2 can be written in integral form as

$$\oint \vec{B} \cdot \vec{n} dS = 0. \tag{3}$$

Remark that Eq. 1 implies that

$$\frac{\partial \nabla \cdot \vec{B}}{\partial t} = 0. \tag{4}$$

The divergence constraint is thus conserved in time on the partial differential equation (PDE) level. This is because the time evolution of $\vec{B}$ is governed by a curl law.

Let us consider three alternative ways in which Eq. 1 can be solved numerically.

First, we can write the curl law as a divergence law using the divergence constraint:

$$\frac{\partial \vec{B}}{\partial t} = -\nabla \cdot (\vec{v}\vec{B} - \vec{B}\vec{v}). \tag{5}$$

This is the standard form of a hyperbolic conservation law. One can use the standard techniques for the numerical solution of hyperbolic conservation laws to discretize this Equation. The $\nabla \cdot \vec{B} = 0$ constraint, however, is violated in general on the discrete level because no special care is taken to conserve it. For smooth flows this does generally not pose significant problems, but at discontinuities large $\nabla \cdot \vec{B}$ errors may arise, which may make numerical schemes unstable.[13–15] One needs to resort to special tricks to resolve this numerical unstability (e.g. the Powell source term[13,14]), but for some flows it remains a problem that the constraint is violated on the discrete level, which may, for instance, result in wrong jumps at discontinuities.[7]

A second way to approach solving Eq. 1 numerically is to rewrite it as a time evolution equation for the magnetic field integrated over a surface S bounded by a closed curve l:

$$\frac{\partial \int \vec{B} \cdot \vec{n} dS}{\partial t} = \oint (\vec{v} \times \vec{B}) \cdot d\vec{l}. \tag{6}$$

The integral quantity in the left hand side of this equation is called the magnetic flux through the bounded surface S. On the discrete level, we can evaluate this formula in terms of the average normal field over the surface S:

$$\int \vec{B} \cdot \vec{n} dS = \bar{B}_n \Delta S. \tag{7}$$

If calculated by Eq. 6, these average normal fields satisfy exactly a discrete divergence constraint, because if we integrate the magnetic flux over a closed surface formed by several discrete surfaces, this closed surface does not have a boundary, such that the right hand side of Eq. 6 vanishes. This is interpreted below as

a consequence of the geometrical property that the boundary of a boundary vanishes. One can also say that the different right hand sides of Eq. 6 cancel out when discrete surfaces are taken together to form a closed surface.

The third way we consider to approach solving Eq. 1 numerically is to rewrite it by introducing the vector potential $\vec{A}$:

$$\vec{B} = \nabla \times \vec{A}, \tag{8}$$

with evolution equation

$$\frac{\partial \vec{A}}{\partial t} = \vec{v} \times (\nabla \times \vec{A}). \tag{9}$$

Londrillo and Del Zanna[6] make the pertinent remark that this is actually a vector Hamilton-Jacobi equation.[16] If we discretize Eq. 9 and calculate $\vec{B}$ from

$$\int \vec{B} \cdot \vec{n} dS = \bar{B}_n \Delta S = \oint \vec{A} \cdot d\vec{l}, \tag{10}$$

then the resulting $\vec{B}$ field is divergence-free at the discrete level, again because the boundary of a boundary vanishes (in Eq. 10).

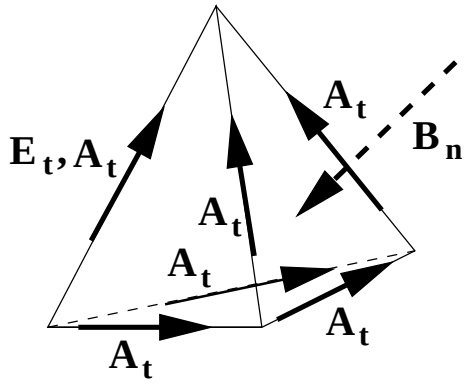

Fig. 1 The components B_n of a divergence-free magnetic field normal to the surfaces of a tetrahedron can be obtained from the tangential components of the vector potential A_t, or the electrical field E_t, along the edges of the tetrahedron.

Let us now investigate what this means for a 3D domain partitioned in non-overlapping tetrahedral cells (Fig. 1). If the temporal evolution of the tangential components of the vector potential A_t can be calculated in some way on the edges of the tetrahedron (Fig. 1) wit the use of Eq. 9, then the components B_n of a divergence-free magnetic field normal to the cell surfaces can be obtained from Eq. 10. Alternatively, the components B_n of a divergence-free magnetic field normal to the cell surfaces can also be updated directly using Eq. 6, if the tangential component of the electrical field $E_t = -(\vec{v} \times \vec{B})_t$ can be established on the edges (Fig. 1) of the tetrahedron.

The constraint-conserving approaches to discretize Eq. 6 for the flux through a surface or Eq. 9 for the vector potential have been explored extensively on structured grids, and have been called 'Constrained Transport' discretizations since they were introduced by Evans and Hawley.[1] However, they have not been explored on unstructured grids, because on unstructured grids it is not immediately obvious how one can reconstruct the full magnetic field vector from its normal components. Indeed, Eq. 6 only gives an evolution equation for the normal components B_n of the magnetic field, whereas the full magnetic field vector $\vec{B}$ is necessary to evaluate its right hand side. The evolution equation for the vector potential Eq. 9 also requires the full magnetic field vector $\vec{B}$ to evaluate its right hand side.

For both cases, however, consideration of so-called 'vector basis functions' or 'edge elements' and 'face elements', to be described in detail below, gives the solution of reconstructing vector fields from components perpendicular to a face or tangential to an edge (see Ref.[17] and references therein). For simulations of the Maxwell equations on unstructured grids these techniques have been used for about ten years by now.[17,18] For MHD or Faraday's equation in the MHD approximation, CT discretizations on unstructured grids using edge and face elements have, to our best knowledge, not been described. They have recently been proposed for the first time by Robinson and Bochev at SANDIA National Laboratories, who are developing CT methods on unstructured grids with quadrilateral elements using classical 1D upwind methods.

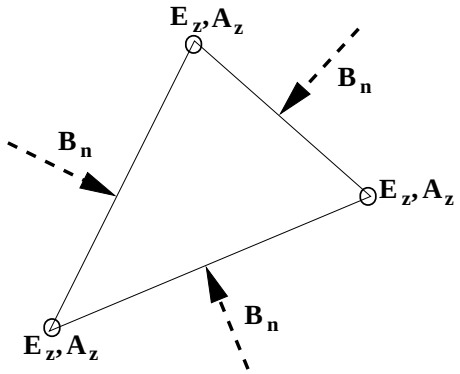

Fig. 2 The components B_n of a divergence-free magnetic field normal to the edges of a triangle can be obtained from the z component of the vector potential A_z, or the z component of the electrical field E_z, in the nodes of the triangle.

In the present paper we combine Multi-dimensional Upwind techniques with a CT face element approach in 2D (we discretize divergence-conserving equations Eq. 6 or Eq. 9), thus obtaining MUCT schemes on 2D triangular unstructured grids. Using the methodology described in this paper the 2D MUCT schemes can easily be generalized to 3D. For now we limit ourselves to the description of MUCT schemes on 2D triangular grids in the xy plane, with $B_z = 0$ and $v_z = 0$ (so-called planar flow). Only the component A_z of the

vector potential is then non-vanishing. On triangles, the edges that contribute to carrying the tangential vector potential component A_z collapse and coincide with the nodes, while the faces that contribute to carrying the xy magnetic field components collapse to the edges of the triangles (Fig. 2). Therefore, in an implementation of CT on a 2D triangular grid, we can store the normal magnetic field components B_n on the edges, and the vector potential A_z in the nodes.

The evolution equation for the normal magnetic field components Eq. 6 now becomes

$$\frac{\partial \int_1^2 \vec{B}\cdot\vec{n}dl}{\partial t} = \frac{\partial \bar{B}_n}{\partial t}\Delta l = (\vec{v}\times\vec{B})_2 - (\vec{v}\times\vec{B})_1, \quad (11)$$

with the integral along a cell edge connecting nodes labeled 1 and 2.

The alternative evolution equation Eq. 9 for the vector potential simplifies to

$$\frac{\partial A_z}{\partial t} = -\vec{v}\cdot\nabla A_z, \quad (12)$$

with the normal magnetic field obtainable from the vector potential as

$$\int_1^2 \vec{B}\cdot\vec{n}dl = \bar{B}_n\Delta l = A_{z,2} - A_{z,1}, \quad (13)$$

the latter relation following from Eq. 10.

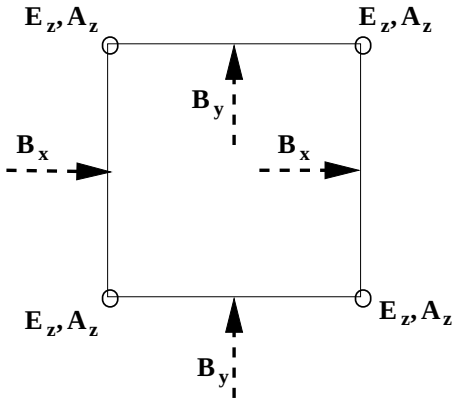

Fig. 3 CT on a regular Cartesian grid.

Fig. 3 shows how CT schemes on regular Cartesian grids are simplified as compared to unstructured grid CT schemes. The normal components of the magnetic field are just the Cartesian components B_x and B_y, which can easily be interpolated to the nodes to provide the magnetic field vector $\vec{B}$ needed to calculate E_z. Face elements are thus not needed to reconstruct the magnetic field. This approach can be generalized to general structured curvi-linear logically rectangular grids using generalized coordinates transformations.[1,7]

A geometrical interpretation

The reason why it is natural to represent the divergence-free magnetic field by its components normal to cell interfaces can be illustrated by considering general concepts from differential geometry, which are sketched in Fig. 4 (see e.g. Ref.,[19] pp. 69–76, for a nice brief introduction with further references). In 3D space, forms — e.g. the 1-form or vector $\omega_1 = A\,dx + B\,dy + C\,dz$ —, are dual to chains — e.g. the 1-chain or line C_1 —, in the sense that the integral of a i-form over a i-chain is a number — e.g. $\int_{C_1}\omega_1$ is the line integral of vector ω_1 along line C_1 (as in the right hand side of Eq. 6). In the same way the flux over a surface is given by $\int_{C_2}\omega_2$ (as in Eq. 7).

For the chains (bottom of Fig. 4), δ is the 'boundary' operator. The boundary of a i-chain is a closed $i-1$-chain: its boundary vasishes. Indeed, the boundary of, e.g., a volume, is a closed surface, and a closed surface does not have a boundary itself! The boundary of a boundary thus vanishes ($\delta^2 \equiv 0$).

For the forms, the exterior derivative d acts as a gradient on a scalar, as a curl on a vector, and as a divergence on a 2-form (or axial vector). Here too, $d^2 \equiv 0$, e.g. $\nabla\times(\nabla\phi) \equiv 0$, and $\nabla\cdot(\nabla\times\vec{A}) \equiv 0$. The gradient of a scalar is a closed vector: its exterior derivative (curl) vanishes. The magnetic field $\vec{B}$ is a closed 2-form: its divergence vanishes. It is the curl of a vector, the vector potential $\vec{A}$. The magnetic field 'geometrically' is not a regular vector, but is an axial vector, or an anti-symmetric 3×3 tensor (which has 3 independent components). An axial vector transforms differently under coordinate transformations than a regular vector.

Edge elements are vector basis functions that describe the vector field in the cell in terms of the vector components tangential to the cell edges. Face elements are (axial) vector basis functions that describe the (axial) vector field in the cell in terms of the (axial) vector components normal to the cell faces.[17] Closed vectors can be represented discretely in a basis of edge elements such that the curl constraint is satisfied everywhere in the cell (see below for examples). Closed 2-forms like the magnetic field can be represented discretely in a basis of face elements such that the divergence constraint is satisfied everywhere in the cell (see below for examples).

Reconstruction of the cell magnetic field using face elements

We consider face elements in triangles.[17] Face elements $\vec{P}_i$ are (axial) vector basis functions with a constant normal component along an edge of the triangle, and vanishing normal component along the two other edges. The (axial) vector field $\vec{B}$ in the cell can then be described in terms of the (axial) vector components normal to the cell faces B_n as

$$\vec{B}_{cell} = \sum_{i=1}^{3} \vec{P}_i\, B_{n,i}, \quad (14)$$

with the sum running over the three cell edges, and the $\vec{P}_i$ the corresponding face vector basis functions with

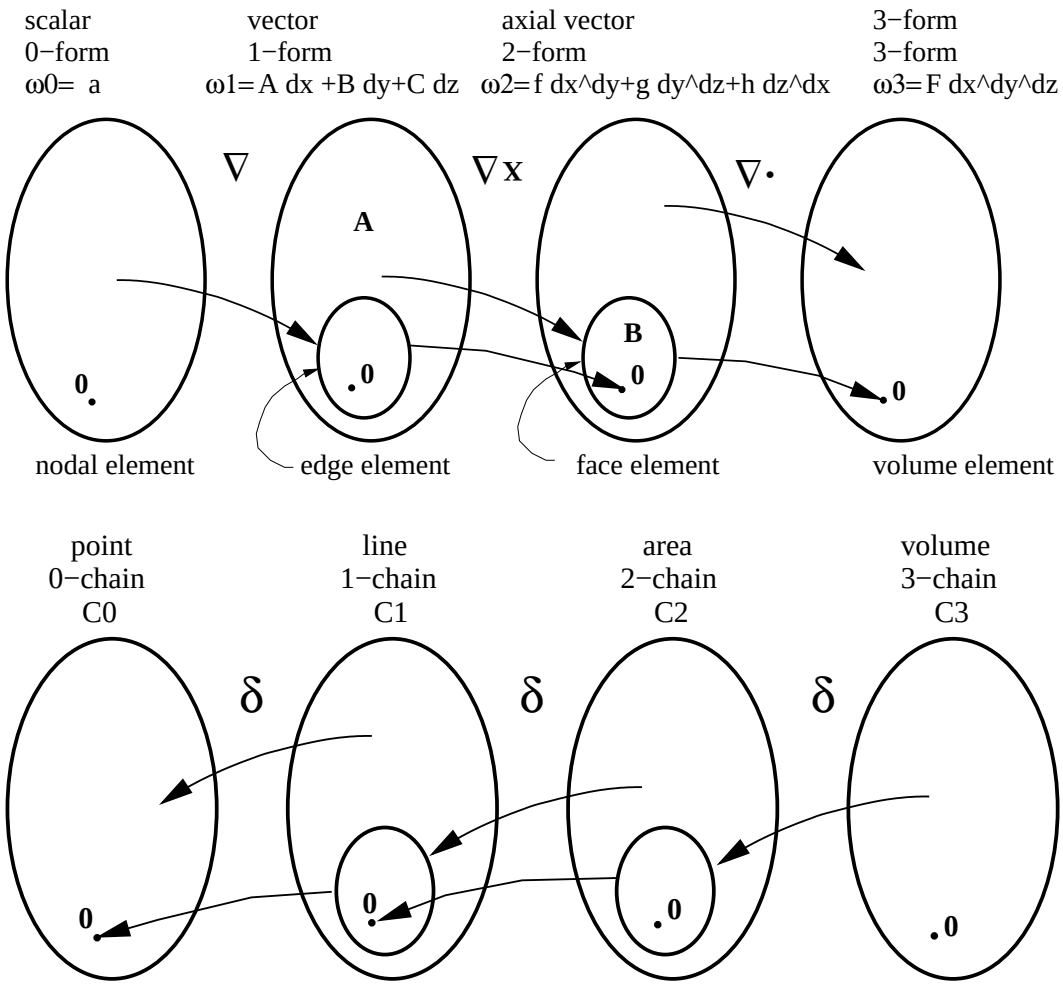

Fig. 4 Concepts from differential geometry. Forms (top) are dual to chains (bottom). For the chains, δ is the 'boundary' operator. The boundary of a i-chain is a closed $i-1$-chain: its boundary vanishes. The boundary of a boundary thus vanishes ($\delta^2 \equiv 0$). For the forms, the exterior derivative d acts as a gradient on a scalar, as a curl on a vector, and as a divergence on a 2-form (or axial vector). Here too, $d^2 \equiv 0$, e.g. $\nabla \times (\nabla \phi) \equiv 0$. The gradient of a scalar is a closed vector: its exterior derivative (curl) vanishes. The magnetic field $\vec{B}$ is a closed 2-form: its divergence vanishes, and it is the curl of a vector, the vector potential $\vec{A}$. The magnetic field 'geometrically' is not a regular vector, but is an axial vector, or an anti-symmetric 3×3 tensor (which has 3 independent components). Closed vectors can be represented discretely by edge elements, and closed 2-forms like the magnetic field can be represented by face elements.

constant normal component along the edges. In Ref.[17] explicit expressions are given for the face elements $\vec{P}_i$ that are derived from linear shape functions L_i, with $L_i = 1$ in node i and $L_i = 0$ in nodes j and k ($i, j, k \in \{1, 2, 3\}$).

The definition of the face elements $\vec{P}_i$ in terms of the geometrical quantities defined in Fig. 5 is

$$\begin{aligned} \vec{P}_1 &= l_1 \, (L_3 \, \nabla \times L_2 - L_2 \, \nabla \times L_3), \\ \vec{P}_2 &= l_2 \, (L_1 \, \nabla \times L_3 - L_3 \, \nabla \times L_1), \\ \vec{P}_3 &= l_3 \, (L_2 \, \nabla \times L_1 - L_1 \, \nabla \times L_2). \end{aligned} \tag{15}$$

Their properties are $\nabla \cdot \vec{P}_i = \textit{constant}$, $\nabla \times \vec{P}_i = 0$, and $\vec{n}_i \cdot \vec{P}_j = \delta_{i,j}$. This justifies expansion Eq. 14, and shows that the divergence of the reconstructed field $\vec{B}$ is constant over the whole triangle. The $\nabla \cdot \vec{B}$ constraint makes that for every triangle there are only two independent $B_{n,i}$ components. This also means that a divergence-free vector field described in a linear face element basis in a triangle is constant over the triangle (since a constant vector has two degrees of freedom). This is also true in a tetrahedron, but not in, e.g., quadrilateral elements.[17] Expressions for face elements for quadrilaterals similar to the expressions in Eq. 15 can be found in Ref.[17]

For curl-free fields, edge elements $\vec{N}_i$ with constant tangential component along one edge and vanishing tangential component along the other edges can be defined,[17] such that a vector field $\vec{E}$ can be expressed in terms of its tangential components at the edges as

$$\vec{E}_{cell} = \sum_{i=1}^{3} \vec{N}_i \, E_{t,i}. \tag{16}$$

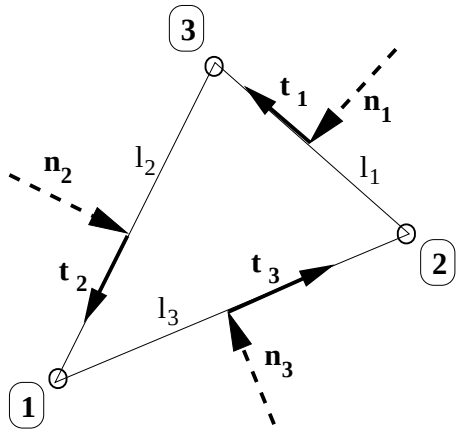

Fig. 5 Notational conventions for normal and tangent vectors and edge and node numbering in a triangle.

We do not need edge elements in the MUCT schemes for 2D problems to be described below.

The edge and face elements described here are also called Nedelec elements or Raviart-Thomas elements.[17] They can be generalized to quadrilaterals.[17]

Multi-Dimensional Upwind Schemes

We give a very brief overview of Multi-dimensional Upwind residual distribution schemes here limited to the case of a scalar advection equation. The reader is refered to Ref.[9] for details and system schemes, which are analogous to scalar schemes.

Given the conservation law

$$\frac{\partial u}{\partial t} + \nabla \cdot f(u) = 0, \tag{17}$$

one defines the cell residual

$$\Phi^T = \int_T \nabla \cdot f(u^h)\, d\Omega, \tag{18}$$

in cell T.

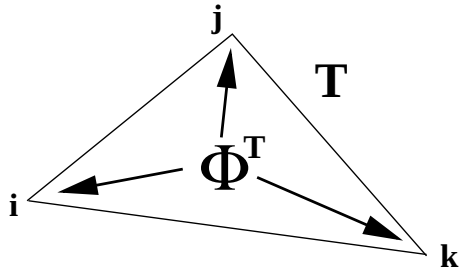

Fig. 6 The cell residual Φ^T is distributed to the nodes u_i of the cell.

The cell residual Φ^T is then distributed to the nodes u_i of the cell as

$$\Phi_i^T = \beta_i^T \Phi^T \tag{19}$$

with $\sum_{i \in T} \beta_i^T = 1$ for conservation (Fig. 6). In a next step the contributions to node i are assembled from all surrounding triangles (Fig. 7), and the nodal value is updated as

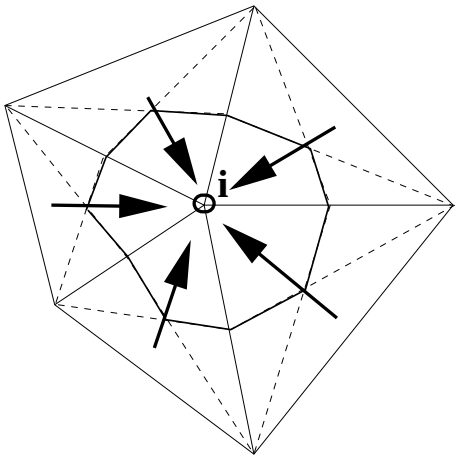

Fig. 7 The contributions to node i are assembled from all surrounding triangles.

$$\frac{\partial u_i}{\partial t} = -\frac{1}{S_i} \sum_{T: i \in T} \beta_i^T \Phi^T, \tag{20}$$

with S_i the area of the median dual cell around node i.

The distribution coefficients β_i are determined such that the resulting scheme is upwind. In quasi-linear form the conservation law reads

$$\frac{\partial u}{\partial t} + \vec{\lambda}(u) \cdot \nabla u = 0. \tag{21}$$

We define the upwind parameters k_i as $k_i = \vec{\lambda}^T \cdot \vec{n}_i/2$ A scheme is called upwind if the residual is distributed to downwind nodes only:

$$\begin{aligned} \Phi_j^T &= 0 \quad \text{when} \quad k_j < 0, \\ \Phi_j^T &\neq 0 \quad \text{when} \quad k_j > 0. \end{aligned} \tag{22}$$

Two cases can be considered: distribution to one target or two targets (Fig. 8). The distribution depends continuously on the direction of the advection vector $\vec{\lambda}$, which means that these schemes are truly Multi-dimensional Upwind.

Many Multi-dimensional Upwind schemes have been proposed; in the present paper we consider the following five schemes.

For the Galerkin or central scheme the distribution coefficients are given by $\beta_i = 1/3$. The Galerkin scheme is unstable for advection.

For the Lax-Wendroff (LW) scheme one chooses $\beta_i = 1/3 + \Delta t/(2S_T)\, k_i$, with S_T the area of the cell. This schemes is second order accurate in space and time, but not positive (or not oscillation-free at discontinuities), and not upwind.

For the LDA scheme the distribution coefficients are given by $\beta_i = k_i^+/(\sum_{m=1}^3 k_m^+)$. This scheme is second

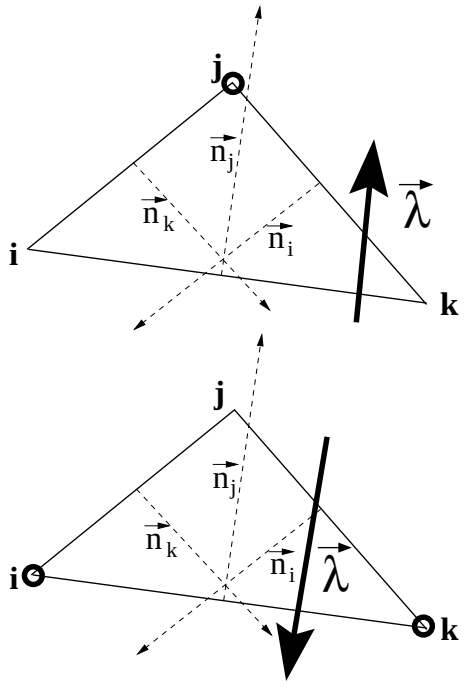

Fig. 8 One-target (top) and two-target (bottom) situations for an upwind scheme.

order in space for steady flow, upwind, but not positive.

For the N scheme $\beta_i = k_i^+ \frac{\sum_j k_j^-(u_i - u_j)}{(\sum_j k_j^-)\,\Phi^T}$. This scheme is only first order accurate, it is positive, and upwind.

The PSI scheme is a limited N scheme.[9] It is second order for steady flow, positive, and upwind.

All these Multi-dimensional Upwind residual distribution schemes are compact on a stencil of nearest neighbors. As in finite volume schemes, it seems to be impossible to obtain second order accuracy in space and time together with positivity on a stencil of nearest neighbors. Space-time schemes allow for second order accurate positive schemes on compact stencils in space, but the stencil has to be extended in time.[9] In the present paper we use the Multi-dimensional Upwind residual distribution schemes as defined above. Our main goal is to describe and illustrate the new MUCT schemes and their performance related to conservation of the $\nabla \cdot \vec{B}$ constraint. In this context the order of accuracy of the discretizations is not of primary concern.

MUCT Schemes for Faraday's equation

MUCT Schemes

We propose two flavors of MUCT schemes for Faraday's equation.

MUCT interpolation schemes for the normal field equations

In the first flavor of 2D MUCT schemes we discretize Eq. 11 using 'Multi-dimensional Upwind' interpolation

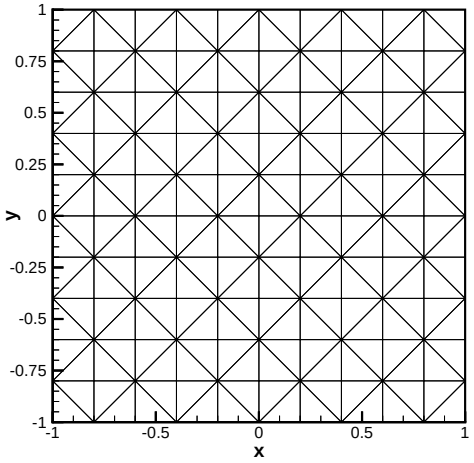

Fig. 9 Unstructured grid of triangles with 11 × 11 nodes.

of the $\vec{B}_{cell,j}$ that surround node i to $\vec{B}$ in node i. We use the Multi-dimensional Upwind interpolation formula given by

$$\vec{B}_i(\sum_{cells j} \beta_j S_{T,j}) = \sum_{cells j} \vec{B}_{cell,j} \beta_j S_{T,j}, \qquad (23)$$

with $S_{T,j}$ the area of cell j. For upwind β_j, this is an upwind-weighted and area-weighted, conservative interpolation. For the distribution coefficients β_j we tried out Galerkin, LW, and LDA, with results to be reported below. The standard Multi-dimensional Upwind residual distribution schemes for advection can thus be reinterpreted as Multi-dimensional Upwind interpolation schemes.

MUCT schemes for the vector potential

In the second flavor of MUCT scheme we solve Eq. 12 using the classical MU schemes (with explicit Euler forward time discretization). This flavor of the MUCT schemes for Faraday's equation simply boils down to the regular scalar MU schemes for the z component of the vector potential A_z.[9] The divergence free magnetic field components normal to the cell edges can then be derived as secondary variables using Eq. 13, and the divergence-free magnetic field can be reconstructed everywhere in the domain using Eq. 14. However, as mentioned before, the magnetic field is constant in every cell, and it turns out that this constant magnetic field in the cell can also be obtained by taking the gradient of the z component of the vector potential A_z assumed to vary linearly over the cell. Face element vector basis functions are thus not necessary in the case of 2D triangulated domains if one solves Eq. 12 directly. In 3D and on quadrilaterals in 2D this simplification does not carry through. We tried all five schemes MU schemes described above, and report on the results below.

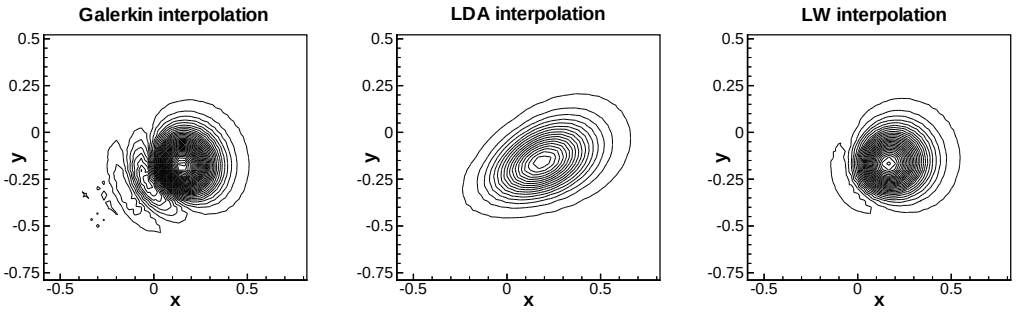

Fig. 10 MUCT interpolation schemes: advection of a Gaussian potential (smooth flow).

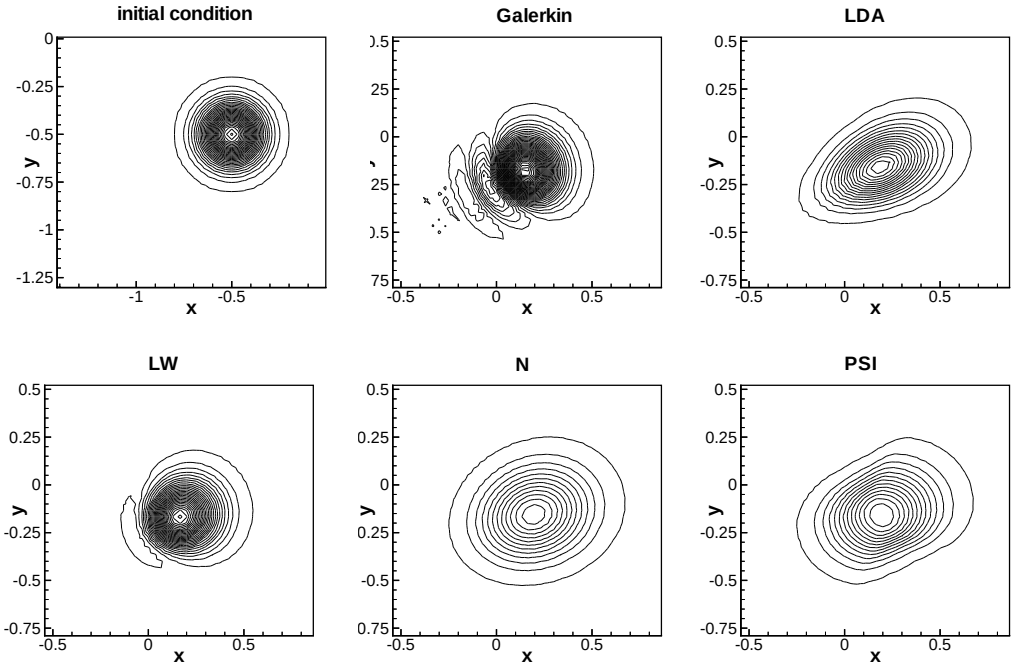

Fig. 11 MUCT schemes for the vector potential: advection of a Gaussian potential (smooth flow).

Model flows

All model flow simulations in the present paper are carried out on grids with the structure of the grid of Fig. 9. This grid of triangles is constructed from an initial structured grid, but it is unstructured and anisotropic because some nodes have four neighboring cells, while other nodes have eight neighboring cells.

We consider two model flows for the MUCT schemes for Faraday's law. In the first model flow the magnetic field derived from a smooth Gaussian potential with expression $A_Z = \exp(-50\,r^2)$, initially centered at position $(x = -0.5, y = -0.5)$, is advected with speed $(vx = 1.0, vy = 0.5)$ for a duration of $t = 0.7$ on a grid with 61×61 nodes.

In the second model flow the magnetic field derived from a discontinuous potential with $A_z = 1$ for $r < 0.25$ and $A_z = 0$ for $r > 0.25$, initially centered at position $(x = -0.5, y = -0.5)$, is advected with speed $(vx = 1.0, vy = 0.5)$ for a duration of $t = 0.7$ on the same grid.

MUCT interpolation schemes for the normal field equations

In Fig. 10 the results of the smooth flow model problem simulated with the MUCT interpolation schemes for the normal field equations are shown. The magnetic field lines are plotted. The Galerkin interpolation creates oscillations. The LDA interpolation diffuses the magnetic field in the direction of the streamlines. The LW interpolation gives a second order accurate solution.

MUCT schemes for the vector potential

In Fig. 11 the results for the simulations with the MUCT schemes for the vector potential are presented. The initial profile is again best preserved by the LW scheme. The Galerkin, LDA and LW are very similar to the results of the MUCT interpolation schemes of Fig. 10. The schemes are almost identical. The N scheme is rather isotropic but diffusive; the PSI scheme suffers from diffusion biased in the streamline direction. Fig. 12 shows how the magnetic energy de-

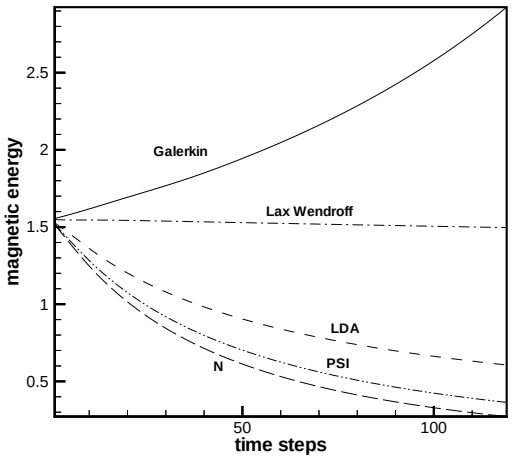

Fig. 12 MUCT schemes for the vector potential: energy dissipation during advection of a Gaussian potential (smooth flow).

cays due to numerical diffusion. The Galerkin scheme is clearly unstable. Only the Lax-Wendroff scheme is second order accurate for this time-dependent flow problem.

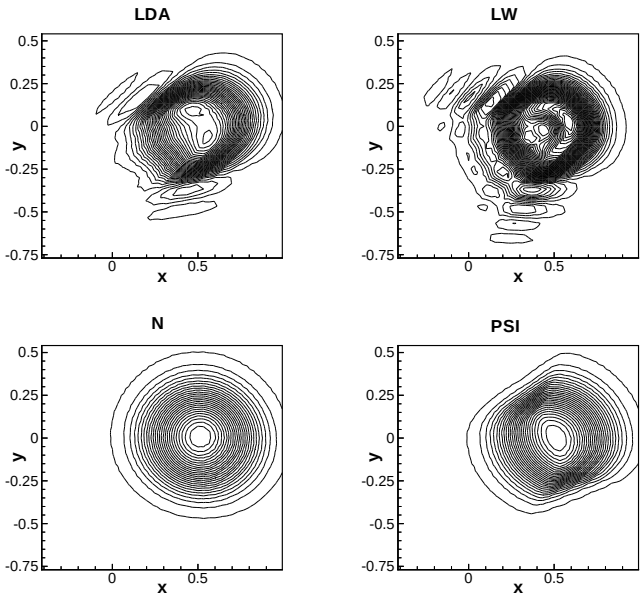

Fig. 13 MUCT schemes for the vector potential: advection of a discontinuous profile.

In Fig. 13 we show the simulation results for the discontinuous profile. Clearly the LDA and LW schemes lose positivity. For discontinuous flow only the N or PSI schemes are viable. Physically one would not directly expect very large gradients in the vector potential to occur in most flows.

Application to the 'Shallow Water' Magnetohydrodynamics Equations

'Shallow Water' Magnetohydrodynamics as a hyperbolic system

Recently the 'Shallow Water' magnetohydrodynamic (SMHD) equations have been proposed[12] for describing the dynamics of nearly incompressible conducting fluids for which the evolution is nearly two-dimensional with magnetohydrostatic equilibrium in the third direction. The SMHD system is a magnetohydrodynamic (MHD) analog to the classical shallow water equations.[20–22] The SMHD equations are presently being used in the study of the dynamics of layers in the solar interior,[23] but they may also be applicable to problems involving the free surface flow of conducting fluids in laboratory and industrial environments.

The properties of SMHD as a hyperbolic system have been discussed extensively by De Sterck in Ref.[24] Here we briefly recapitulate the expressions that are relevant for the derivation of MUCT schemes for the SMHD equations as discussed below.

The equations of SMHD[12] describing the temporal evolution of the primitive variables $\mathbf{V} = (h, v_x, v_y, B_x, B_y)^T$ are given by

$$\begin{aligned} \frac{\partial h}{\partial t} + \nabla \cdot (h\,\vec{v}) &= 0, \\ \frac{\partial \vec{v}}{\partial t} + (\vec{v}\cdot\nabla)\vec{v} - (\vec{B}\cdot\nabla)\vec{B} + g\,\nabla h &= 0, \\ \frac{\partial \vec{B}}{\partial t} + (\vec{v}\cdot\nabla)\vec{B} - (\vec{B}\cdot\nabla)\vec{v} &= 0, \\ \nabla \cdot (h\,\vec{B}) &= 0. \end{aligned} \qquad (24)$$

Here h is the height of the conducting fluid, v_x and v_y are the components of the fluid velocity vector $\vec{v}$, and B_x and B_y are the components of the magnetic field vector $\vec{B}$. These five state variables are functions of time t and spatial coordinates x and y. The parameter g is the magnitude of the gravitational acceleration. The evolution equations are supplemented with a divergence constraint $\nabla \cdot (h\vec{B}) = 0$. The evolution equations are such that this constraint remains automatically satisfied at later times if it is satisfied at an initial time.

As is shown by Gilman,[12] the SMHD equations (24) can be derived from the full MHD equations by integration in the z direction under the assumptions of incompressibility, 2D variation of the flow variables,

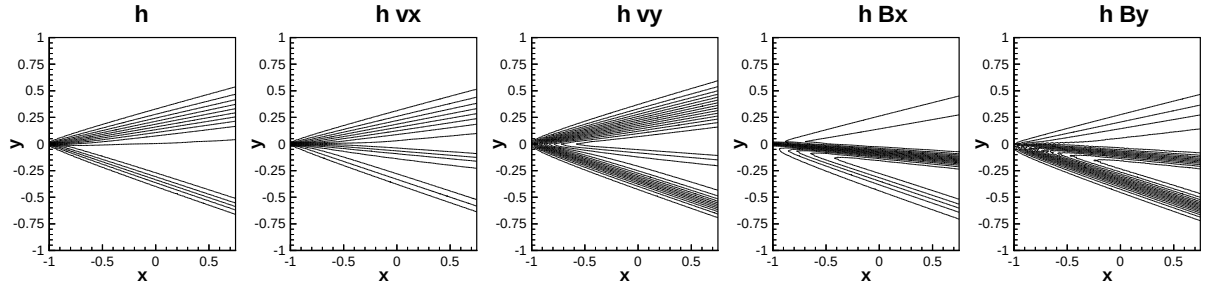

Fig. 14 System N MUCT solution of the steady Riemann problem on a grid of 91×91 nodes.

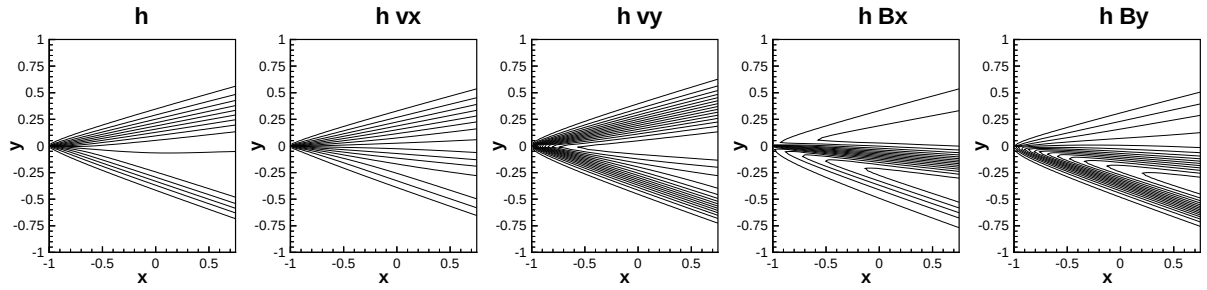

Fig. 15 First order Lax-Friedrichs finite volume solution of the steady Riemann problem on a grid of 90×90 finite volumes.

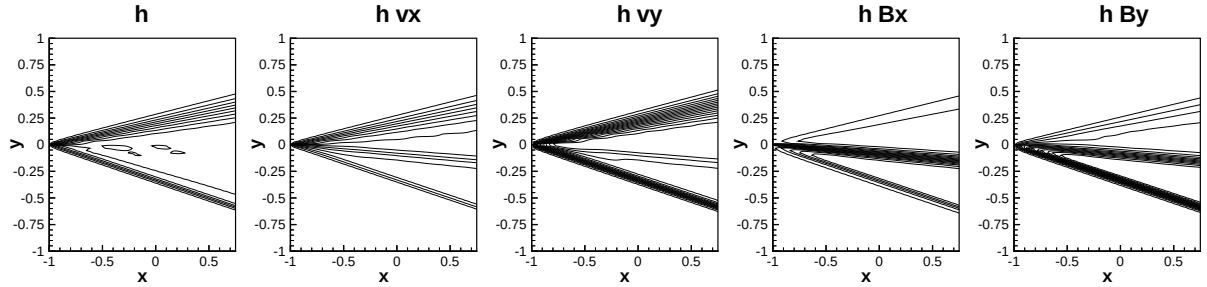

Fig. 16 Second order Lax-Friedrichs finite volume solution of the steady Riemann problem on a grid of 90×90 finite volumes.

and magnetohydrostatic equilibrium in the z direction:

$$\frac{\partial}{\partial z}\left(p + \frac{B^2}{2}\right) = \rho\, g,$$
$$p + \frac{B^2}{2} = \rho\, g\, z,$$
$$\int_0^h \left(p + \frac{B^2}{2}\right) dz = \rho\, g\, \frac{h^2}{2}. \qquad (25)$$

The derivation of SMHD from MHD is analogous to the derivation of the shallow water equations from the Euler equations.[21]

Using the $\nabla \cdot (h\vec{B}) = 0$ constraint, the SMHD equations (24) can be recast in the form of a system of conservation laws, as a function of the conserved variables $\mathbf{U} = (h, m_x, m_y, \phi_x, \phi_y)^T = (h, h\,v_x, h\,v_y, h\,B_x, h\,B_y)^T$:

$$\frac{\partial}{\partial t}\begin{bmatrix} h \\ h\,\vec{v} \\ h\vec{B} \end{bmatrix} + \nabla \cdot \begin{bmatrix} h\,\vec{v} \\ h\,\vec{v}\vec{v} - h\,\vec{B}\vec{B} + \mathsf{I}\left(gh^2/2\right) \\ h\vec{v}\vec{B} - h\vec{B}\vec{v} \end{bmatrix} = 0. \qquad (26)$$

Tensor notation is used here, with for instance the i,jth component of $\vec{B}\vec{v}$ given by $(\vec{B}\vec{v})_{i,j} = v_i\, B_j$. This form of the equations explicitly shows that the temporal variation of the conserved quantities is balanced by the divergence of a flux.

Four wave modes are described by the SMHD equations. The eigenvalues of the Jacobian are given by

$$\lambda_{1,2} = v_x \mp c_{ax}, \quad \lambda_{3,4} = v_x \mp c_{gx}, \quad \lambda_5 = v_x, \quad (27)$$

with

$$c_{ax} = B_x, \qquad (28)$$
$$c_{gx} = \sqrt{B_x^2 + g\,h}. \qquad (29)$$

The fifth wave is a spurious wave (the $\nabla \cdot \vec{B}$-wave[13,14]).

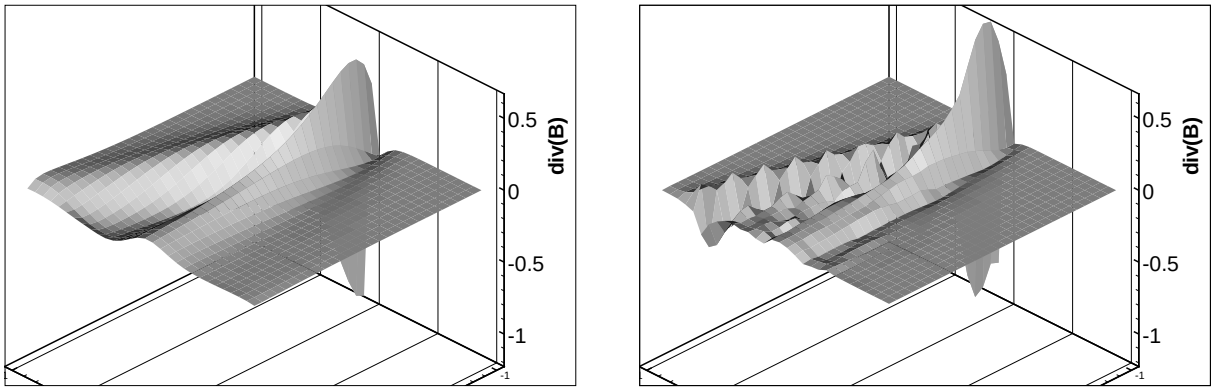

Fig. 17 $\nabla \cdot \vec{B}$ **for the first order (left) and second order (right) Lax-Friedrichs simulation of the steady Riemann problem on a grid of** 30×30 **finite volumes.**

The columns $\mathbf{R}_i$ of matrix

$$\mathsf{R} = \left[\begin{array}{c|c|c|c|c} 0 & 0 & -h & -h & B_x \\ 0 & 0 & \sqrt{B_x^2 + g\,h} & -\sqrt{B_x^2 + g\,h} & 0 \\ 1 & -1 & 0 & 0 & 0 \\ 0 & 0 & B_x & B_x & g \\ 1 & 1 & 0 & 0 & 0 \end{array}\right] \tag{30}$$

are the right eigenvectors of the Jacobian, and describe the properties of the SMHD waves.

Wave modes 1 and 2 are called Alfvén waves due to their close resemblance to the MHD Alfvén waves. As can be seen from inspecting $\mathbf{R}_1$ and $\mathbf{R}_2$, the Alfvén waves carry only perturbations in v_y and B_y, the vector components perpendicular to the direction of propagation.

Wave modes 3 and 4 are gravity waves that are modified by magnetic forces, and are called magneto-gravity waves. They carry perturbations in the longitudinal field components, and in the height.

SMHD wave modes 1, 2 and 5 are linearly degenerate waves, as $\nabla\lambda_1 \cdot \mathbf{R}_1 \equiv 0$, $\nabla\lambda_2 \cdot \mathbf{R}_2 \equiv 0$ and $\nabla\lambda_5 \cdot \mathbf{R}_5 \equiv 0$. The magneto-gravity modes, however, are genuinely nonlinear, as $\nabla\lambda_3 \cdot \mathbf{R}_3 = 3\,g\,h\,/(2\,\sqrt{B_x^2 + g\,h}) \neq 0$ and $\nabla\lambda_4 \cdot \mathbf{R}_4 = -3\,g\,h\,/(2\,\sqrt{B_x^2 + g\,h}) \neq 0$. Compressional magneto-gravity modes can thus steepen into shocks. It is important to note that $\nabla\lambda_3 \cdot \mathbf{R}_3$ and $\nabla\lambda_4 \cdot \mathbf{R}_4$ do not change sign, which means that modes 3 and 4 are convex modes, such that compound shocks do not occur.[21] This is in contrast to the fast and slow MHD waves, which are nonconvex,[25–27] such that compound shocks occur in MHD flows.

MUCT schemes for SMHD

MUCT schemes for the SMHD equations can be obtained by combining Multi-dimensional Upwind residual distribution schemes for the full SMHD system with updating the normal magnetic field components or the nodal vector potentials as in Eqs. 11 or 12. In what follows we employ the system N scheme[9] and we discretize the vector potential equation Eq. 12.

From the vector potential A_z we derive the divergence free magnetic field components normal to the cell edges using Eq. 13, and the cell divergence-free magnetic field is derived using Eq. 14. The cell magnetic fields are then interpolated to the nodes using Eq. 23 with the Galerkin central distribution coefficients $\beta_i = 1/3$. These nodal magnetic fields are used by the system N scheme to update the other variables.

Following this nodal update the vector potential A_z is advected using the scalar N scheme, with the cell advection velocity determined by the average of the nodal velocities. This constitutes the system N MUCT scheme employed in the simulations below.

Model flows

We impose a supersonic horizontal field-aligned inflow on the left boundary of the domain in Fig. 14, with $h = 2$, $v_x = 5.5$, $v_y = 0$, $B_x = 0.5$ and $B_y = 0$ on the upper half of the left boundary, and with $h = 1$, $v_x = 4.5$, $v_y = 0$, $B_x = 2.$ and $B_y = 0$ on the lower half of the left boundary.

Figs. 14, 15 and 16 show the steady state simulation results of the resulting steady Riemann problem flow for the new MUCT scheme, and for first order and second order Lax-Friedrichs finite volume schemes (without CT).[15] It can be seen that the discontinuous inflow at the left boundary results in, from bottom to top, a shock, a contact Alfvén discontinuity, and a rarefaction. The results obtained by the three schemes agree well. We have to remark that for many flow problems, including this Riemann problem, it does not make so much difference for the global solution whether we impose the divergence-free constraint up to machine accuracy or not. For other problems, however, it has been shown that very significant differences may arise.[7] It is our aim to verify in this steady Riemann model flow if we reach our goal of obtaining a MUCT solution with a divergence-free magnetic field up to machine accuracy on unstructured grids.

Figs. 17 and 18 show the $\nabla \cdot \vec{B}$ plots for the simulation results. Fig. 17 shows how $\nabla \cdot \vec{B}$ is generated by the finite volume schemes. The order of magnitude of the $\nabla \cdot \vec{B}$ generated is similar to the $\nabla \cdot \vec{B}$ generated with the traditional full system N scheme without

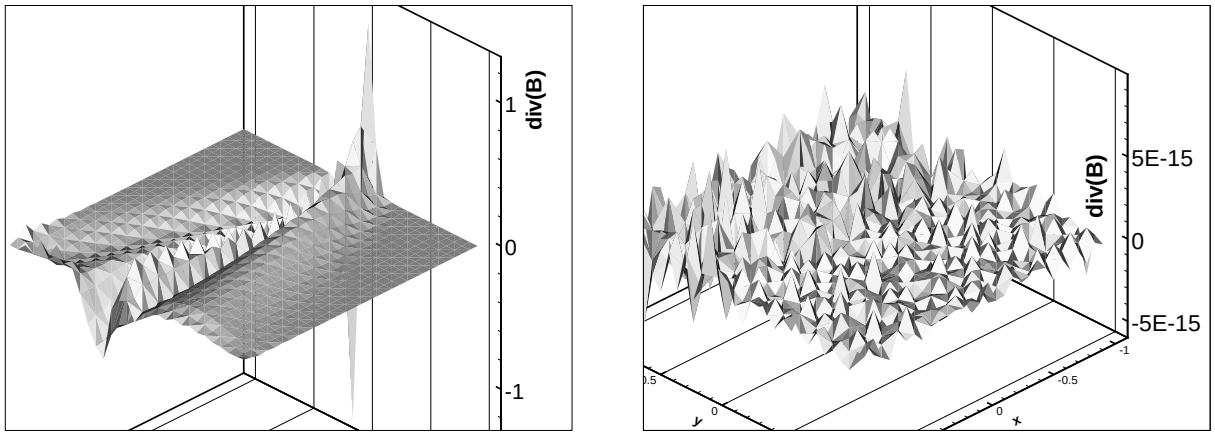

Fig. 18 $\nabla \cdot \vec{B}$ **for the full system N (left) and system N MUCT (right) simulation of the steady Riemann problem on a grid of** 31×31 **nodes.**

CT[11,28] as shown in the left panel of Fig. 18. The result obtained by the new MUCT system N scheme satisfies the $\nabla \cdot \vec{B} = 0$ constraint up to machine accuracy (see the right panel of Fig. 18).

Conclusions

Novel Multi-dimensional Upwind Constrained Transport (MUCT) schemes on unstructured triangular grids were described. These schemes are obtained by combining the concept of Constrained Transport, generalized to unstructured triangular grids using face elements, with the concept of Multi-dimensional Upwind advection schemes. It was shown how a system N MUCT scheme can be designed capable of obtaining numerical flow solutions of Shallow Water MHD flows with a divergence-free magnetic field up to machine accuracy on unstructured grids. More accurate MUCT schemes based on sytem PSI or system B schemes[9] can be formulated in a completely analogous fashion.

Using the methodology described in this paper the 2D MUCT schemes presented can easily be generalized to 3D. The MUCT schemes can be applied to any hyperbolic system with divergence-free fields, including the full MHD equations. In the MUCT schemes the CT approach is generalized to multi-dimensional methods on unstructured grids.

Acknowledgments

I thank H. Deconinck for teaching me his insights in the Multi-dimensional Upwind methodology. P. Bochev and A. Robinson are acknowledged for pointing me to the concepts of edge and face elements for MHD Constrained Transport on unstructured grids.

This research was carried out in the framework of the projects OT/98/14 (K.U. Leuven), G.0344.98 (FWO Vlaanderen), and 14815/00/NL/SFe(IC) (ESA Prodex).

References

[1]Evans, C. R. and Hawley, J. F., "Simulation of magnetohydrodynamic flows: a constrained transport method," *Astrophys. J.*, Vol. 332, 1988, pp. 659–677.

[2]Stone, J. M. and Norman, M. L., "ZEUS-2D: A radiation magnetohydrodynamics code for astrophysical flows in two space dimensions. II. The magnetohydrodynamic algorithms and tests," *Astrophys. J. Suppl.*, Vol. 80, 1992, pp. 791–818.

[3]Ryu, D., Miniati, F., Jones, T. W., and Frank, A., "A Divergence-free Upwind Code for Multidimensional Magnetohydrodynamic Flows," *Astrophys. J.*, Vol. 509, 1998, pp. 244–255.

[4]Dai, W. and Woodward, P. R., "On the divergence-free condition and conservation laws in numerical simulations for supersonic magnetohydrodynamic flows," *Astrophys. J.*, Vol. 494, 1998, pp. 317–335.

[5]Balsara, D. S. and Spicer, D. S., "A staggered mesh algorithm using high order Godunov fluxes to ensure solenoidal magnetic fields in magnetohydrodynamic simulations," *J. Comput. Phys.*, Vol. 149, 1999, pp. 270–292.

[6]Londrillo, P. and Zanna, L. D., "High-order upwind schemes for multi-dimensional magnetohydrodynamics," *Astrophys. J.*, Vol. 530, 2000, pp. 508–524.

[7]Toth, G., "The $\nabla \cdot \vec{B} = 0$ constraint in shock-capturing magnetohydrodynamics codes," *J. Comput. Phys.*, Vol. 161, 2000, pp. 605–652.

[8]Deconinck, H., Roe, P. L., and Struijs, R., "A multidimensional generalization of Roe's flux difference splitter for the Euler equations," *J. Comp. Fluids*, Vol. 22, 1993, pp. 215–222.

[9]Deconinck, H., Sermeus, K., and Abgrall, R., "Status of multidimensional upwind residual distribution schemes and applications in aeronautics," *AIAA* Paper 2000-2328, 2000.

[10]van der Weide, E., Deconinck, H., Issman, E., and Degrez, G., "A parallel, implicit, multi-dimensional upwind, residual distribution method for the Navier-Stokes equations on unstructured grids," *Computational Mechanics*, Vol. 23, 1999, pp. 199–208.

[11]Csík, A., De Sterck, H., van der Holst, B., Deconinck, H., and Poedts, S.,"Parallel Residual Distribution Solver for the 3D Magnetohydrodynamics Equations: Applications to Flows in Space Physics," *AIAA* Paper 2001-2622, 2001.

[12]Gilman, P. A., "MHD 'shallow water' equations for the solar tachocline," *Astrophys. J. Letters*, Vol. 544, 2000, p. L79.

[13]Powell, K., "An approximate Riemann solver for magnetohydrodynamics (that works in more than one dimension)," Tech. Rep. 94-24, ICASE Langley, VA, 1994.

[14]Powell, K. G., Roe, P. L., Linde, T. J., Gombosi, T. I., and De Zeeuw, D. L., "A solution-adaptive upwind scheme for magnetohydrodynamics," *J. Comput. Phys.*, Vol. 154, 1999, p. 284.

[15]De Sterck, H., Csik, A., Vanden Abeele, D., Poedts, S., and Deconinck, H., "Stationary two-dimensional magnetohydrodynamic flows with shocks: characteristic analysis and grid convergence study," *J. Comput. Phys.*, Vol. 166, 2001, p. 28.

[16]Barth, T. J. and Sethian, J. A., "Numerical schemes for the Hamilton-Jacobi and level set equations on triangulated domains," *J. Comput. Phys.*, Vol. 145, 1998, pp. 1–40.

[17]Jin, J., *The finite element method in electromagnetics*, Wiley-Interscience, New York, 1993.

[18]Bochev, P., Hu, J., Robinson, A. J., and Tuminaro, R., "Towards robust 3D Z-pinch simulations: discretization and fast solvers for magnetic diffusion in heterogeneous conductors," Tech. Rep. SAND Report 2001-8363J, Sandia National Laboratories, 2001.

[19]Ryder, L. H., *Quantum field theory*, Cambridge University Press, Cambridge, 1996.

[20]Stoker, J. J., *Water Waves*, Interscience, New York, 1957.

[21]Leveque, R. J., *Numerical methods for conservation laws*, Lectures in Mathematics ETH Zurich, Birkhauser-Verlag, Basel, 1992.

[22]Toro, E. F., *Shock-Capturing Methods for Free Surface Shallow Fluids*, John Wiley and Sons, New York, 2001.

[23]Dikpati, M. and Gilman, P. A., "Prolateness of the solar tachocline inferred from latitudinal force balance in a magnetohydrodynamic shallow water model," *Astrophys. J.*, Vol. 552, 2001, p. 348.

[24]De Sterck, H., "Hyperbolic theory of the shallow water magnetohydrodynamics equations," *Phys. Plasmas*, 2001, in press.

[25]Brio, M. and Wu, C. C., "An upwind differencing scheme for the equations of ideal magnetohydrodynamics," *J. Comput. Phys.*, Vol. 75, 1988, pp. 400–422.

[26]De Sterck, H., *Numerical simulation and analysis of magnetically dominated MHD bow shock flows with applications in space physics*, Ph.D. thesis, Katholieke Universiteit Leuven, Belgium, and National Center for Atmospheric Research, Boulder, Colorado, USA, 1999.

[27]De Sterck, H., Low, B. C., and Poedts, S., "Characteristic analysis of a complex two-dimensional magnetohydrodynamic bow shock flow with steady compound shocks," *Phys. Plasmas*, Vol. 6, No. 3, 1999, pp. 954–969.

[28]Csik, A., Deconinck, H., and Poedts, S., "Monotone residual distribution schemes for the ideal 2D magnetohydrodynamic equations on unstructured grids," *AIAA* Paper 99–3325, 1999.